Journal of Colloid and Interface Science 638 (2023) 569–581

Contents lists available at ScienceDirect

Journal of Colloid and Interface Science

journal homepage: www.elsevier.com/locate/jcis

Surface stress decomposition in large amplitude oscillatory interfacial dilatation of complex interfaces

Anteun de Groot [a], Jack Yang [a,b], Leonard M.C. Sagis [a,*]

[a] Laboratory of Physics and Physical Chemistry of Foods, Wageningen University, Bornse Weilanden 9, 6708WG Wageningen, The Netherlands
[b] Laboratory of Biobased Chemistry and Technology, Wageningen University, Bornse Weilanden 9, 6708 WG Wageningen, The Netherlands

HIGHLIGHTS

- A stress decomposition of dilatational stress responses including physical interpretations.
- Complex interfaces show network and surface density effects in their stress response to large oscillatory amplitude dilatation.
- A way to quantify the asymmetry and nonlinearity of stress responses and to relate this to the interface.

GRAPHICAL ABSTRACT

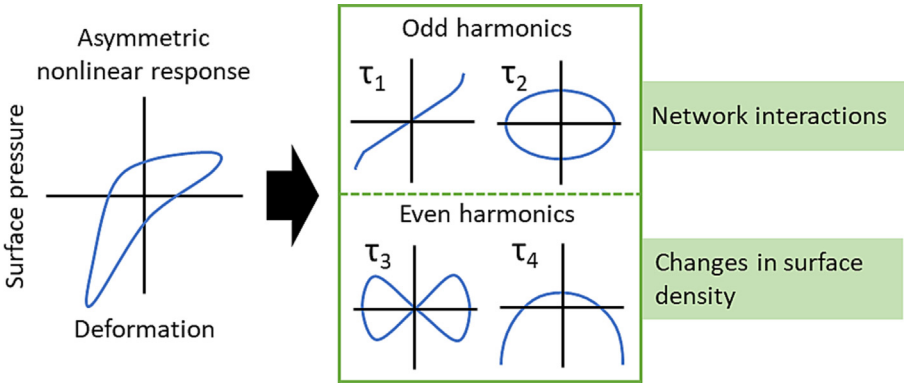

ARTICLE INFO

Article history:
Received 24 November 2022
Revised 1 February 2023
Accepted 1 February 2023
Available online 4 February 2023

Keywords:
Interfacial rheology
Stress decomposition
Lissajous plots
Large amplitude oscillatory dilatation
Complex interfaces
Multiphase materials

ABSTRACT

Hypothesis: Multiphase materials are often subjected to large deformations during processing, but the rheological responses of complex interfaces (e.g. stabilized by proteins) in this nonlinear deformation regime are still poorly understood. We expect nonlinearities in the response to be introduce by changes of the interfacial network and surface density of the emulsifier.

Experiments: Large amplitude oscillatory dilatation (LAOD) experiments were performed on WPI-, pea albumin-, pea globulin- and rapeseed lecithin-stabilized interfaces and analyzed with a general stress decomposition (GSD). With GSD, the stress response was decomposed into the four stress terms (τ_1-τ_4). Here, τ_1 and τ_2 represent, the elastic and viscous contribution of the odd Fourier harmonics, and τ_3 and τ_4 represent the dissipative and recoverable contribution of the even harmonics.

Findings: Analysis of WPI-, pea albumin-, pea globulin- and rapeseed lecithin-stabilized interfaces revealed that higher odd harmonics ($k \geq 3$) describe in-plane network responses and that even harmonics describe surface density changes. Analysis of these complex interfaces showed that GSD is a valuable tool for (quantitative) description of interfacial responses in LAOD, providing new insights into the origin of asymmetric nonlinear stress responses.

1. Introduction

Multiphase dispersed systems (e.g. emulsions, foam, biological fluids) are found in a wide variety of applications, from food and cosmetics to living organisms [1–3]. Such systems have multiple

* Corresponding author.
E-mail address: leonard.sagis@wur.nl (L.M.C. Sagis).

https://doi.org/10.1016/j.jcis.2023.02.007
0021-9797/

immiscible phases (e.g. water and oil) and typically have a large surface area separating the phases. The formation and stability of these systems can be significantly influenced by the interfacial rheological properties, such as the interfacial shear and dilatational modulus and viscosity. [1,4–6]. This has resulted in numerous studies on the interfacial properties of multiphase dispersed systems in the last decades [1,4–12].

The response of interfacial layers is often viscoelastic, and their rheology, in particular dilatational rheology, is often studied assuming a *linear* viscoelastic (LVE) response. In the LVE regime, the stress response to a sinusoidal deformation is a single sine function, shifted in time. The Fourier spectrum of the stress shows only a single harmonic at the applied frequency. Linearity might be a reasonable assumption for interfaces stabilized by low molecular weight surfactants, for which the response (upon deformation) is dominated by exchange of surfactants between bulk and interface [13,14]. However, this assumption is generally not valid for interface stabilizers that form viscoelastic layers with strong in-plane interactions among absorbed stabilizers [14]. The typical strain range applied in interfacial studies using tensiometers varies between 1 and 10 %, and such strains often already introduce nonlinearities [7,10,15–17], resulting in a response in the nonlinear viscoelastic (NLVE) regime.

Strain amplitude sweeps can be used to assess whether the experiments are performed in the LVE regime. However, such tests are still rarely performed in dilatational surface rheology. At low strains, complex interfaces (e.g. stabilized by proteins or nanoparticles) show solid-like viscoelastic behavior [16,18–21], which suggests the stabilizers are in an aggregated or jammed state. When sufficiently large amplitudes are applied, this microstructure will be disrupted [21], resulting in an asymmetric nonlinear stress response with a different response in extension and compression [20]. The asymmetry is problematic for the analysis of the interfacial response in terms of dilatational moduli. Dilatational moduli are typically calculated by Fourier transformation of the surface pressure signal, from which the amplitude and phase of the first harmonic are extracted [8,10–12,22]. Nonlinearities in the response lead to the emergence of higher harmonics [20,23], and in the calculation of first harmonic-based moduli, valuable information contained in these higher harmonics is neglected. As interfaces in multiphase systems are often subjected to large deformations during processing or use, this information is important to assess. Solid-like interfacial layers may yield when they are highly deformed, resulting in substantial softening, which can lead to significant differences between the static and dynamic stability of a system.

Lissajous plots have been introduced as a tool to visualize nonlinear viscoelastic responses [13,24]. Lissajous plots are cyclic curves constructed by directly plotting the surface pressure at every time t versus deformation. The surface pressure, $\Pi(t)$, is related to the surface tension $\gamma(t)$ by:

$$\Pi = \gamma - \gamma_0 \tag{1}$$

Here, γ_0 is the surface tension of the non-deformed interface. Lissajous curves can be used to visualize the contributions of the higher harmonics to an interfacial stress response, as shown in Fig. 1. In the LVE regime, the surface pressure is identical at equal compression or expansion, but of the opposite sign. This results in Lissajous plots which are symmetric with respect to the origin. In the NLVE regime the interface can have a different response in expansion than in compression, and we often see strain softening in expansion and strain hardening in compression (Fig. 1). Although Lissajous plots provide a good visualization of nonlinear and asymmetric interfacial stress responses, a systematic and quantitative interpretation of nonlinear Lissajous plots remains challenging. For oscillatory shear measurements on bulk samples, extensive schemes exist to quantify Lissajous plots, for example, through stress decomposition, or calculation of the energy dissipation ratio [25,26]. Similar schemes for asymmetric dilatational responses have received only limited attention [13,27].

The novelty of the work presented here is that we provide a new method to quantify the nonlinear responses in dilatational rheology, based on stress decomposition, which allows us to introduce several new quantitative measures. These can subsequently be used to quantitatively compare the responses of several complex interfaces. More precisely, we quantify nonlinear asymmetric responses in dilatational rheology by a decomposition of the surface pressure into four distinct contributions (two containing only

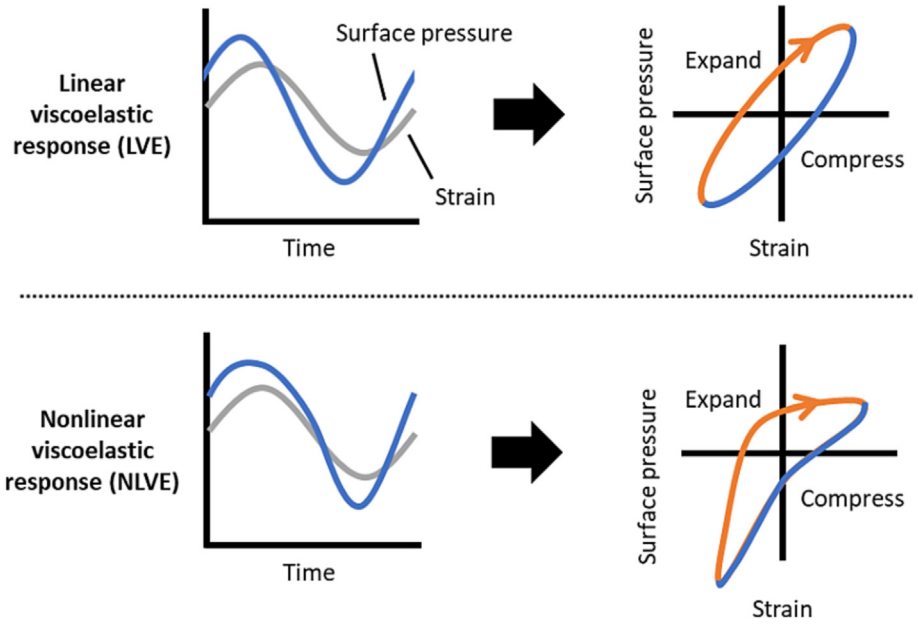

Fig. 1. The construction of Lissajous plots for a viscoelastic response in the linear and nonlinear viscoelastic regime. Lissajous plots for dilatational rheology in the nonlinear regime exhibit a different response in expansion than in compression.

odd harmonics, and two containing only even harmonics), as previously suggested by Bykov et al. (2015). In section 2, we provide the theoretical background for this general stress decomposition. We then apply this decomposition to interfacial films stabilized by various interfacial stabilizers (whey protein, pea proteins, rapeseed lecithin), and provide a physical interpretation of the four stress contributions (an issue that was not yet fully addressed). We then introduce several measures, for each of the four stress components, which can be used to quantitatively distinguish systems. Analyzing the responses of interfaces using this novel method provides additional insight into the physical processes, which are occurring at interfaces during deformation, and will help us to better understand the link between surface properties and macroscopic stability of multiphase systems.

2. Theoretical background

2.1. Lissajous plots

Lissajous plots are a qualitative and accurate method to analyze nonlinear stress responses. In dilatational rheology, these plots can be constructed by plotting the oscillating surface pressure signal against deformation, and this yields several typical responses, shown in Fig. 2. In Fig. 2 A, the response of an interface with completely elastic behavior is shown, where all the applied energy is stored upon deformation. In plot B, purely viscous behavior is shown, and the applied energy is completely dissipated. Generally, the linear viscoelastic (LVE) response of an interface is a combination of A and B, resulting in a response as shown in plot C. The ellipse shape results from a summation of an elastic and a viscous contribution. Within the nonlinear viscoelastic (NLVE) regime shear responses show a 'distorted' ellipsoidal shape, e.g. rhomboidal as shown in plot D. Whereas, large amplitude oscillatory dilatation (LAOD) in the NLVE regime can yield a stress with a magnitude that is direction dependent, resulting in the asymmetric nonlinear response shown in plot E. A different response is obtained in expansion (upper part of the cycle, from bottom left to top right) and compression (the lower part of the cycle, from top right to bottom left).

2.2. Shear surface rheology

To better understand the origin of the asymmetries observed in the nonlinear response in dilatational rheology, it is helpful to first consider the stress responses in surface shear experiments. The response to shear can be described by a Fourier series which contains only odd harmonics (i.e. sines and cosines with only odd multiples of the applied frequency). As a result, the Lissajous plots of the stress (in shear rheology) are symmetric with respect to the origin [28–30]. The reason for this symmetry is that the shear response should be independent of the direction of shear, i.e. clockwise and counterclockwise rotations should give an identical response (if the system is isotropic).

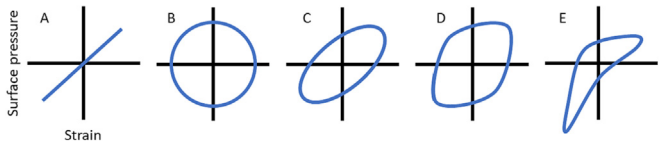

Fig. 2. Lissajous plots of surface pressure (or stress) versus strain. (A) Purely elastic response; (B) Purely viscous response; (C) Linear viscoelastic response; (D) nonlinear response in shear rheology; (E) nonlinear asymmetric response in dilatational rheology.

Shear strain sweeps performed on interfaces stabilized by components with strong in-plane interactions often show Lissajous plots with a narrow ellipsoidal shape in the linear viscoelastic regime, which suggests a solid-like viscoelastic response dominated by the elastic component. At higher deformation amplitudes (Fig. 2 D), the response becomes nonlinear. This is manifested as a transition to more open and rhomboidal shaped plots. The increase in width of the cycle indicates an increase of the viscous contribution to the stress, and the rhomboidal shape indicates (partial) intra-cycle yielding, followed by flowing of the interfacial microstructure. At maximum positive and negative strain (where the strain rate is zero), the interfacial microstructure can (partially) recover. This leads to a cyclic sequence of elastic response (the near vertical parts of the loop), yielding (the upper left and lower right corners), flow (the horizontal parts of the loop), and recovery (upper right and lower left corners). Later in this work, we will refer to this behavior to explain the asymmetries in the interfacial response in dilatation.

Lissajous plots in shear rheology are often quantified by, for instance, determining the energy dissipation ratio, or through stress decomposition [26]. These analyses are relatively easy to perform in shear due to the symmetric shape. However, in dilatational (surface) rheology, the asymmetry of the Lissajous plots complicates a similar analysis. In further sections, we explain the origin of the asymmetry and suggest a methodology to overcome these problems and quantify dilatational Lissajous plots.

2.3. General stress decomposition

We will now consider the response of interfaces to a dilatational deformation, with a sinusoidal strain of the form $\varepsilon = \varepsilon_0 \sin(\omega t)$, where ε_0 is the deformation amplitude, ω is the applied angular frequency, and t is time. In the NLVE regime, this response can again be described by a Fourier series, so a summation of multiple waves (Eq. (2)), but which now contains both even and odd harmonics.

$$\Pi(t) = \sum_{k=0}^{\infty} q_k sin(k\omega t + \delta_k) \tag{2}$$

Here q_k is the amplitude, and d_k is the phase shift of the k^{th} harmonic, respectively. Equation (2) can be decomposed into a sum of odd and even sine and cosine functions, given by

$$\Pi(t) = \tau_1 + \tau_2 + \tau_3 + \tau_4 \tag{3}$$

The stresses τ_i (i = 1–4) are equal to

$$\tau_1 = \sum_{k=0}^{\infty} b'_{2k+1} sin((2k+1)\omega t) \tag{4}$$

$$\tau_2 = \sum_{k=0}^{\infty} a'_{2k+1} cos((2k+1)\omega t) \tag{5}$$

$$\tau_3 = \sum_{k=0}^{\infty} c'_{2k} sin(2k\omega t) \tag{6}$$

$$\tau_4 = \sum_{k=0}^{\infty} d'_{2k} cos(2k\omega t) \tag{7}$$

The definitions of τ_1 – τ_4 are identical to the ones proposed by Yu et. al (2009), who described a method to decompose a general Fourier series into four individual contributions (τ_1, τ_2, τ_3, τ_4), based on symmetry transformations [31].

The coefficients a'_{2k+1} and b'_{2k+1} are the coefficients of the odd harmonics, and c'_{2k} and d'_{2k} are the coefficients of the even harmonics. The phase shift of odd harmonics is described by $\delta_{2k+1} = \tan^{-1}\left(\frac{a'_{2k+1}}{b'_{2k+1}}\right)$ and the phase shift of the even harmonics is equal to $\delta_{2k} = \tan^{-1}\left(\frac{d'_{2k}}{c'_{2k}}\right)$.

The dilatational response decomposes into four contributions because of the asymmetry between the compression and extension part of the cycle. For surface shear responses, only τ_1 and τ_2 would be present in the signal, and there they represent the elastic and viscous contributions to the stress, respectively [23,25,27]. Any nonlinearities in these terms are typically linked to changes/disruptions of the microstructure of the system, especially at large deformations. We would expect these contributions to be dominant for surface-active components, which display strong in-plane interactions among adsorbed stabilizers and, as a result, associate into solid-like interfacial microstructures. The contribution of nonlinearities might already be present at small amplitude deformations but is often still reflected as (near) symmetric Lissajous plots. This is confirmed in several studies, where near symmetric plots are obtained at low amplitudes [8–12,32,33].

The asymmetries in large amplitude dilatation are introduced by τ_3 and τ_4, and since in these stress contributions the leading oscillatory contribution has frequency 2ω, these plots are symmetric with respect to the vertical axis. Large amplitude dilatations will not only disrupt the microstructure of an interface. In addition, significant surface density changes during the oscillation cycle are expected for surface-active components that adsorb irreversibly at the interface, or when the period of oscillation is shorter than the time scale for exchange between the bulk and interface phase. In both cases, the surface density decreases in expansion and increases in compression of the interfacial area. Therefore, we would expect the asymmetries introduced by τ_3 and τ_4 to be related to the surface density changes during deformation. Just like for the odd harmonics, τ_3 represents a dissipative (i.e. viscous) contribution and τ_4 a reversible (i.e. elastic) contribution to this additional stress contribution. In the next sections, we will examine the exact nature of these stress contributions in more detail and introduce several new measures to quantify them.

3. Materials & methods

Yellow pea (Pisum Sativum L.) seeds were obtained from Alimex Europe BV (Sint Kruis, The Netherlands), rapeseed phospholipids (commercial lecithin) from Cargill (Emulphur RS Lecithin, France) and whey protein isolate (WPI) from Davisco Food international (BiPro, France). All other chemicals (Sigma-Aldrich, USA) were used as received. MilliQ water (Ultrapure lab, Germany) was used in all experiments.

3.1. Sample preparation

Pea albumin and globulin were obtained as described by Kornet et al. (2022) [34]. Pea albumin and globulin were dissolved to a concentration of 0.1 % (w/w) protein in a sodium phosphate buffer (20 mM, pH 7.0).

Whey protein isolate (WPI) was dissolved at 2.5 % protein (w/w) and stirred for 4 h in sodium phosphate buffer. The solution was centrifuged at 16,000xg for 30 min and filtered through a 0.45 μm syringe membrane filter. The filtrate was subsequently diluted based on dry matter content to 0.1 % (w/w).

Rapeseed lecithin was dispersed in sodium phosphate buffer for 2 h at room temperature under constant stirring. High-speed mixing was used at 8,000 rpm for 10 s with an Ultra-Turrax (IKA, USA), and the sample was left overnight at 4 ^{0}C to hydrate.

All samples were freshly prepared for all measurements and discarded after 24 hrs.

3.2. Dilatational analysis

Interfacial properties of air–water interfaces stabilized by pea globulin and pea albumin were determined with a drop tensiometer PAT-1 M (Sinterface Technologies, Germany) at a concentration of 0.1 % protein (w/w). A hanging droplet of 20 mm^2 was formed, and the shape was analyzed with the Young-Laplace equation to determine the surface tension. Before dilating the droplet, the area was maintained at 20 mm^2 for 3 hrs. Amplitude sweeps were performed at an increasing amplitude from 5 to 30 % at 0.02 Hz.

Measurements on air–water interfaces stabilized by WPI and Lecithin were performed with an ADT (Teclis, France) at 0.1 % (w/w), which was operated similarly to the PAT. Instead of 20 mm^2, a hanging droplet area of 15 mm^2 was used at the tip of a G18 needle. Amplitude sweeps (5–60 %) were performed after 3 h of waiting time, at a frequency of 0.02 Hz.

Each amplitude within the sweep consisted of five oscillatory cycles, of which the middle three oscillations were used for analysis. Between the series of oscillations, the interface is left to equilibrate for 50 s, whereafter the next cycle of oscillations is performed. The measurements were performed at least in triplicate at room temperature.

3.3. Analysis of higher harmonics from dilatational rheology

The construction of Lissajous plots and the contributions of higher harmonics were analyzed in a MATLAB (R2020b) script. The script calculates the surface tension, γ_0, from the surface tension before and after an oscillation to adjust for baseline shifting. For the last cycle of oscillations only the surface tension before oscillation was used since the experiments stopped directly after this cycle. With γ_0 the surface pressure is now calculated according to Eq. (1). For each strain amplitude, the middle three oscillations of each cycle of five are selected, and for these the strain and stress are interpolated over one period, followed by a fast Fourier transformation. From the Fourier transform of the interpolated signal only the first 10 harmonics were included for further calculations, to suppress random noise.

Strain is applied according to $\varepsilon = \varepsilon_0 \sin(\omega t)$, so only the first harmonic of its Fourier transform is used to reconstruct the smoothed strain.

The script also calculates all relevant measures we introduced in the main text of this manuscript. We developed a custom MATLAB app based on this script which is available upon request by contacting the corresponding author.

3.4. Statistical analysis

Standard deviation is calculated for all samples from three individual measurements. Significant differences are determined with a two-tailed students' *t*-test and a significance level of $p < 0.05$.

4. Results & discussion

4.1. General stress decomposition of a constructed sinusoid

For the sake of simplicity, the concept behind the general stress decomposition (GSD, introduced in Eq. (3)) and the result after applying the GSD will first be illustrated by applying it to a constructed sinusoidal signal, which contains both odd and even harmonics, and arbitrary amplitudes and phase shifts (i.e. an arbitrary example of Eq. (2)):

$$\Pi(t) = sin(2\pi t + 0.2\pi) - 0.18sin(2 * 2\pi t - 0.22\pi) - 0.15sin(3 * 2\pi t - 0.2\pi) + 0.04sin(4 * 2\pi t + 0.4\pi) + 0.05sin(5 * 2\pi t + 0.2\pi) + 0.01sin(6 * 2\pi t + 0.5\pi) \quad (8)$$

This constructed stress response is somewhat similar to a response previously observed in dilatational rheology of WPI-stabilized interfaces [10,16,35–37]. The applied strain was sinusoidal, with $\varepsilon(t) = \varepsilon_0 \sin(2\pi t)$ with strain amplitude ε_0. The leading harmonic has a fundamental frequency of 2π s^{-1} and higher harmonics have a frequency of $2k\pi$ s^{-1} with k being the k^{th} harmonic. The Lissajous plot of Eq. (8) is given in Fig. 3A. At the start of expansion (lower-left corner of the plot), the curve has a steep slope, which for a real interface would indicate a high stiffness. As the expansion proceeds, we observe a gradual decrease in the slope of the curve, which we have previously identified as a gradual yielding of the interfacial microstructure, finally leading to intracycle strain softening. In the compression part of this cycle, we see a gradual increase in slope of the curve for negative strain, and the surface stress at maximum compression is clearly higher than the stress at maximum expansion. This behavior has been referred to as strain hardening (in the context of our studies on WPI). Since the response in expansion is different from compression, the response is clearly asymmetric.

To gain a better understanding of the origin of the behavior described by Eq. (8), we applied the GSD to this signal, and plotted the individual τ-terms versus deformation $\varepsilon(t)$ in Fig. 3 B1, B2, C1 and *C2*, with the stresses associated with the odd harmonics ($\tau_1 + \tau_2$) in plot B and the stresses associated with the even harmonics ($\tau_3 + \tau_4$) in plot C. The individual contribution of τ_1 and τ_2 are similar to what was previously obtained in the decomposition of the stress signal in shear rheology of bulk phases [28,30,38]. In our example, the elastic stress τ_1 (Fig. 3 B1) is given by an inverted sigmoidal curve, and the plot of τ_2 (Fig. 3 B2) has a spherical shape that is flattened around zero strain (where the strain rate is at a maximum). Combining τ_1 and τ_2 results in a symmetric rhomboidal shape (plot B). In shear rheology, such a shape indicates a gradual transition to plastic behavior [28]. Like in the parental curve (Fig. 3 A), the curve is steep in the initial phase of the extension cycle, indicating high interfacial stiffness. This is followed by a significant change in slope, indicating yielding of the microstructure. The fact that τ_1 (Fig. 3 B1) still has a finite slope around zero strain indicates only partial disruption of the microstructure. For a particulate gel, this would imply partial break down of particle clusters, and the upswing at maximum strain (a mild intracycle strain hardening) is often associated with stretching of residual (intact) clusters. For such a system, the flattening of the circular curve for τ_2 (Fig. 3 B2) around zero strain, or maximum strain rate, could be a sign of shear thinning during the flow phase of the structure, but can also be associated with relaxation phenomena occurring on the same timescale as the timescale of the cycle.

The contributions of τ_3 and τ_4 are represented by a lemniscate-shaped (or infinity-shaped) curve (Fig. 3C1) and a single curved line (Fig. 3 C2), respectively. Combining these signals resulted in a skewed infinity-shaped curve (Fig. 3 C). The infinity-shaped loop of τ_3 indicates energy dissipation, and the single curved line for τ_4 indicates energy storage. From this decomposition of the signal in Fig. 3 A, the even harmonics clearly are the only contributor to the asymmetry of the plot. By isolating the even harmonics with the GSD, we can now study them in more detail to interpret their physical meaning.

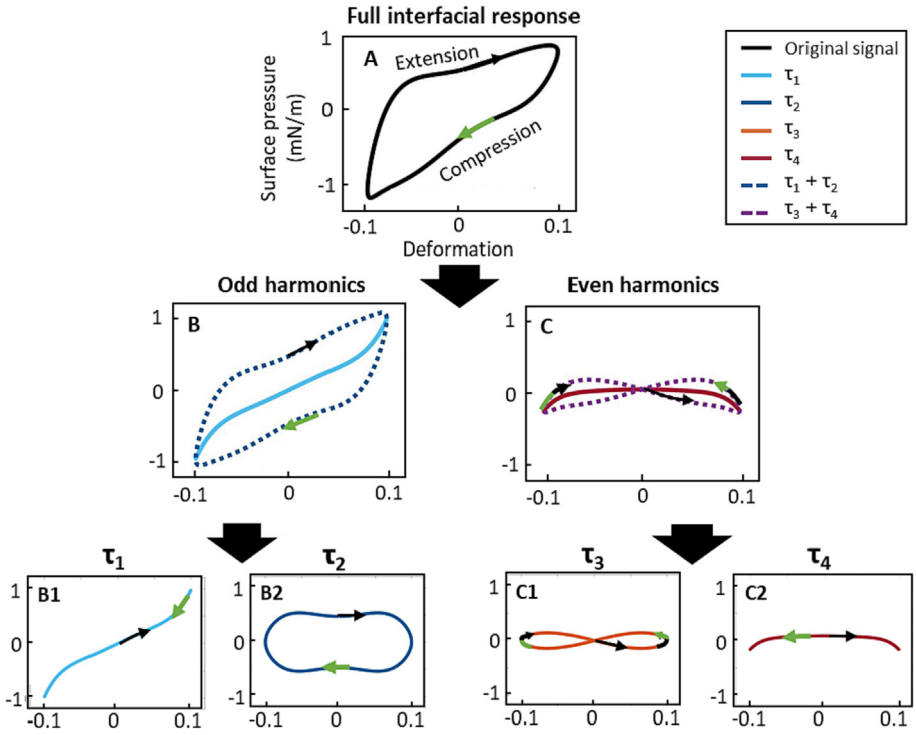

Fig. 3. Lissajous plot of a constructed sinusoidal surface pressure signal (A, Eq. (8)) decomposed into a contribution from the odd harmonics (dark blue, dashed) with its elastic contribution (blue, line) (B); and a contribution from the even harmonics (purple, dashed) with its elastic contribution (red, line) (C). The odd harmonics are further decomposed in τ_1 (B1, blue) and τ_2 (B2, dark blue) and the even harmonics in τ_3 (C1, orange pink) and τ_4 (*C2*, red). The direction of the cyclic deformation is indicated with orange arrows in extension and with blue arrows in compression. (For interpretation of the references to colour in this figure legend, the reader is referred to the web version of this article.)

4.2. GSD for WPI-stabilized interfaces

We will now apply the GSD to dilatational stress responses of several real systems and will particularly focus on systems for which it is well-established that they form solid-like viscoelastic structures after adsorption at air–water or oil–water interfaces. We start with WPI-stabilized air–water interfaces, which show asymmetric Lissajous plots in large amplitude dilatation, as confirmed by several studies [16,32,33]. The asymmetry would indicate a significant contribution of even harmonics at large deformations. This is confirmed in Fig. 4, where at the largest deformations (30–60 %), we see a considerable contribution from τ_3 and τ_4 to the overall stress. At 5 % deformation (Fig. 4 A-D), a symmetric Lissajous plot is obtained, where the first (odd) harmonic alone describes the interfacial response (Fig. 4B), and the contributions from the even harmonics are negligible (Fig. 4 C, D). At larger deformations, the Lissajous plots of the WPI-stabilized interfaces showed a clear asymmetry. This was most evident at 60 % deformation (Fig. 4 M), where we observed an intracycle yielding response in the initial expansion phase, followed by a strain softening in the final phase. In addition, a mild strain hardening is shown in compression. This asymmetry is clearly the result of the substantial contribution of the even harmonics, which is also reflected as larger signals for τ_3 and τ_4 in Fig. 4 O, P. In previous work, the main component in WPI, β-lactoglobulin (BLG), was found to self-associate after adsorption to the interface and formed solid viscoelastic interfacial films. A combination of atomic force microscopy, dilatational frequency sweeps, and step dilatational measurements has shown that the most likely structure BLG (and hence WPI) forms at the interface is a disordered solid, which is either a 2D particle gel or jammed particle system [16].

For bulk protein particle gels in shear, we also see symmetric ellipsoid-shaped Lissajous plots at small deformation amplitudes, and then a gradual transition to rhomboidal-shaped plots which are associated with (partial) disruption of the gel network [26]. In view of the similarity of shear plots to the stress contribution from the odd harmonics ($\tau_1 + \tau_2$) in LAOD, and the fact that the protein appears to form a particulate viscoelastic solid at the interface, it appears reasonable to assume a similar origin of the odd harmonics in dilatational rheology. Therefore, the rhomboidal-shaped plots for $\tau_1 + \tau_2$ are the results of the gradual disruption of a 2D protein particle network. To understand how such effects end up in a surface pressure signal, we closely examine the Laplace equation used for its determination, or rather, the surface momentum balance it is based on. When in-plane inertial stresses, viscous and inertial stresses exerted on the interface by the adjoining bulk phases, and contributions from bending rigidity are all negligible, the surface momentum balance reduces to Eq. (9), as shown in [39]:

$$\Delta P\boldsymbol{n} = 2\gamma H\boldsymbol{n} + \nabla_s \cdot \boldsymbol{\sigma}^s \tag{9}$$

Here, ΔP denotes the pressure difference across the interface, H is the curvature of the interface, $\boldsymbol{n}$ is the unit normal vector, and $\nabla_s \cdot \boldsymbol{\sigma}^s$ is the surface divergence of the surface stress tensor. This last term describes in-plane deviatoric stresses generated by deformation of the microstructure of the interface. For a near spherical geometry, like the one used in a droplet tensiometer, we can approximate this term by $2H(\mathrm{tr}\boldsymbol{\sigma}^s)\boldsymbol{n}$, where $\mathrm{tr}\boldsymbol{\sigma}^s$ denotes the trace of the surface stress tensor. With this approximation, Eq. (9) reduces to

$$\Delta P = 2\gamma_{eff} H \text{ with } \gamma_{eff} = \gamma + tr\sigma^s \tag{10}$$

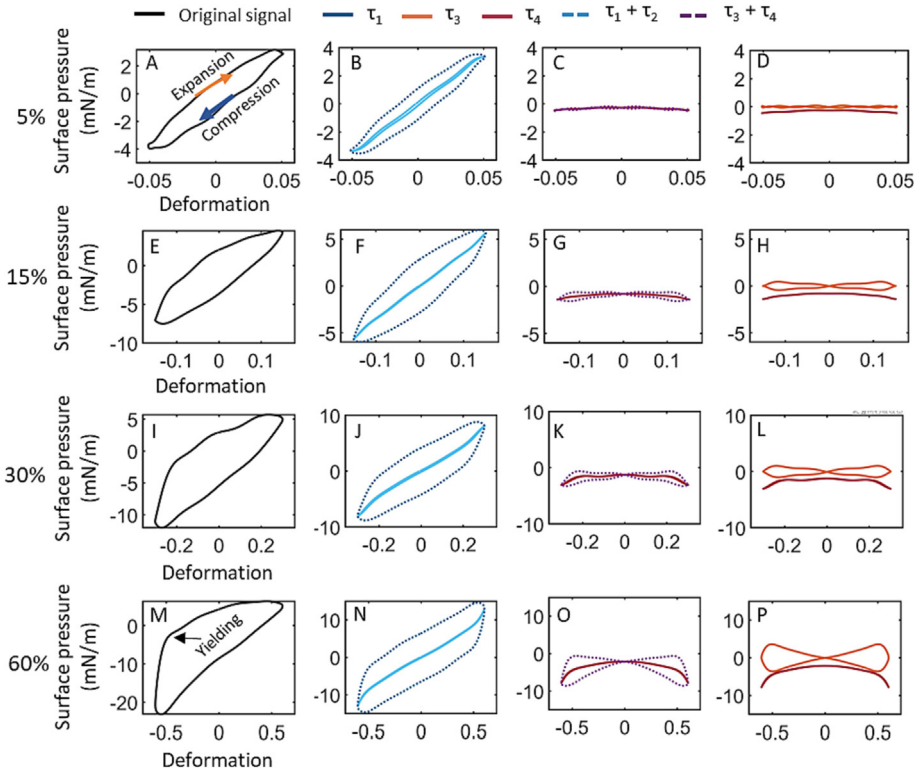

Fig. 4. The (decomposed) Lissajous plots of WPI-stabilized air–water interfaces (0.1 % w/w), at an oscillation amplitude of 5 %, 15 %, 30 % and 60 %. The original signal is shown in plot A, E, I, M (black, line), τ_1 (blue, line) and $\tau_1 + \tau_2$ (blue, dashed) in plot B, F, J, N, τ_4 (red, line) and $\tau_3 + \tau_4$ (purple, dashed) in plot C, G, K, O, and τ_3 (orange, line) and τ_4 (red, line) are given in plot D, H, L, P,. (For interpretation of the references to colour in this figure legend, the reader is referred to the web version of this article.)

So, we see that for complex interfaces, we actually determine an effective surface pressure, which contains a contribution of the dynamic surface tension and from deviatoric stresses. The latter contributions are responsible for the nonlinearities in the response, and would be absent for simple interfaces, such as those stabilized by low molecular weight surfactants. For these types of interfaces, $\tau_1 + \tau_2$ would have an ellipsoidal shape.

Let us now turn to the even harmonics (τ_3 and τ_4) in Fig. 4. The even harmonics in dilatation are present only in the nonlinear regime, where large amplitudes are applied. Apart from disrupting the 2D structure of an interface, dilatational deformations also change the surface coverage of a surface-active stabilizer, when it is (partially) irreversibly adsorbed (on the timescale of the oscillation). As noted earlier, expansions will then lead to a decrease in surface density, whereas compressions will increase surface density. This is especially relevant for interfacial films, where the adsorbed stabilizers have strong in-plane interactions, since these can limit the mass exchange between interface and bulk upon deformation. These changes in surface density will affect the surface pressure: according to Eq. (1), they will increase the surface pressure in expansion and decrease it (i.e. make it more negative) in compression.

To illustrate how surface density changes lead to the specific form of τ_4, let us consider a specific example. In the absence of any deviatoric contributions, and any diffusional exchange between interface and bulk, the overall stress curve would follow the surface pressure-area isotherm. The simplest form of that isotherm is that of an ideal surface gas (illustrated in Fig. 5 A),

$$\gamma - \gamma_c = nRT/A \tag{11}$$

Here, γ_c is the surface tension of the clean interface, n is the number of moles of the surface-active component adsorbed at the interface, R is the gas constant, T is the temperature, and A is the surface area. This isotherm is nonlinear in the area, and it would give a curved line in the Lissajous plot (Fig. 5 B). Applying the GSD to such a curve will give a contribution for τ_1 (Fig. 5 C, a straight line) and a contribution for τ_4 (Fig. 5 D) which accounts for the difference between the straight line for τ_1 and the actual curve for the total stress as indicated in Fig. 5 A & B. Upon expansion, we see that τ_4 becomes increasingly negative, until maximum expansion is reached, and then increases again along the same curve upon compression. For negative strains, the curve is a mirror image of the curve for positive strains.

If there is diffusional exchange present, the plot in Fig. 5 B would take on a bent ellipsoidal shape [1,4–12,40], and there will also be contributions from the dissipative stresses τ_2 and τ_3. So, the even harmonics appear to be associated with nonlinearities of γ in the equation of state of the interface.

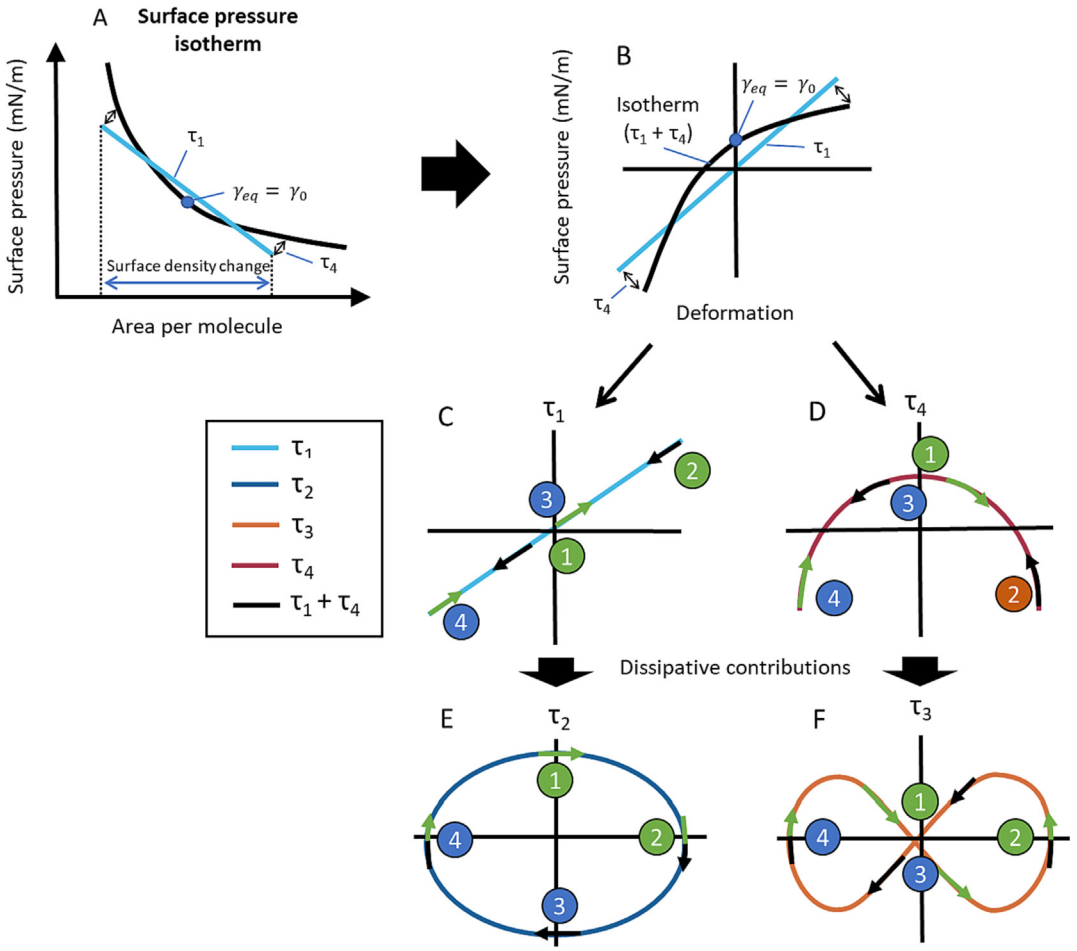

Fig. 5. The surface pressure isotherm (A) with the corresponding elastic Lissajous plot of surface pressure versus deformation (B). The elastic Lissajous plot consists of a contribution of the first odd harmonic contained in τ1 (C) and a contribution of τ4 (D), which can be extracted with our decomposition. If the response is viscoelastic also dissipative contributions described by τ2 (E) and τ3 (F) appear. The typical Lissajous plots for τ1 (B), τ2 (E), τ3 (F) and τ4 (D) have arrows showing the direction of deformation; in extension arrows are orange, and in compression arrows are blue. The numbers correspond to key moments during a deformation cycle, 1: expansion at 0 deformation, 2: maximum expansion, 3: compression at 0 deformation, 4: maximum compression. (For interpretation of the references to colour in this figure legend, the reader is referred to the web version of this article.)

The typical shape of τ_1 – τ_4 is shown in Fig. 5 C – F, along with the direction of the curve. For τ_1 and τ_2, we see an elastic and viscous contribution that is also observed in shear rheology. For τ_4, an additional thing we notice is that in general this stress is not centered with respect to the horizontal axis, and the average of τ_4 is negative (Fig. 4 L & P). This shift is an indication that we are oscillating around a non-equilibrium state, with $\gamma_0 \neq \gamma_{eq}$, and causes an overall shift (γ_s) of the total stress with respect to the horizontal axis, yielding

$$\gamma_{eq} = \gamma_0 + \gamma_s \tag{12}$$

So our analysis suggests that the higher odd harmonics in the stress response are the result of changes in the in-plane network structure, and the even harmonics are associated with nonlinearities in the equation of state of the interface. But we need to point out that this separation of network and density effects only applies for isotropic interfaces, in which the equation of state is a smoothly decreasing function with increasing surface area (i.e. $\partial\gamma/\partial A < 0$and $\partial^2\gamma/\partial A^2 > 0$). For interfaces with an anisotropic network structure, nonlinearities in the deviatoric stresses may generate even harmonics [41]. And when the surface isotherm has an inflection point, density changes may generate odd contributions to the surface stress.

We can now associate the different interactions to the response described by Eq. (13), which is a simple rearrangement of Eq. (3).

$$\gamma_{eff} = \gamma_1 + \sum_{k=1}^{\infty}\gamma_{2k+1} + \sum_{k=1}^{\infty}\gamma_{2k} + \gamma_s \tag{13}$$

Here, γ_1 is the first odd harmonic from which the well-known E'$_d$ & E"$_d$ are normally determined. The term, $\sum_{k=1}^{\infty}\gamma_{2k+1}$ is the sum of all higher odd harmonics contained in τ_1 and τ_2, describing the the contributions due to changes in the interfacial microstructure. And $\sum_{k=1}^{\infty}\gamma_{2k}$ is the sum of all higher even harmonics (contained in τ_3 and τ_4) describing the nonlinearities in the equation of state.

This new analysis of the stress response of an air–water interface stabilized by WPI, based on the GSD, provides an alternative explanation for the asymmetric Lissajous plots of WPI-stabilized interfaces in dilatation. Previously, we attributed the shape of the plot in Fig. 4 M, in which we see initially a stiff response in expansion, followed by intra-cycle yielding, and a completely flat curve in the final stages of expansion, as a complete breakdown of interfacial structure, followed by flow [16,35–37]. However, when the GSD is applied to the stress signals at high amplitude, a rhomboidal shaped curve is observed for the odd harmonics (τ_1 + τ_2, Fig. 4 N), with an inverted sigmoidal elastic contribution (τ_1). The finite slope at zero deformation indicates that the interfacial network is still (partly) intact, even at the largest amplitude of 60 %. Strain hardening of the elastic contribution near the extremes of deformation indicates a residual network that is being stretched. The flattening of the total stress curve near maximum extension in Fig. 4 M is caused by the even harmonics (τ_3 + τ_4), and hence related to changes in the surface density of the interface. On an intracycle level, the GSD allows us to decouple the nonlinear contributions to the total surface stress from network disruption and changes in surface density, leading to a better understanding of the dynamics of this complex interface.

4.3. General stress decomposition for several other interfacial stabilizers

In this section, we compare the GSD for WPI-stabilized interfaces with the GSD for several other interfaces, such as air–water interfaces stabilized by pea globulin, pea albumin and lecithin, at 30 % deformation (Fig. 6). Pea globulins and albumins are two different plant protein classes. Pea globulins are generally large proteins with molecular weights varying from 170 to 380 kDa and may even exist in a larger aggregated state. Pea albumins are substantially smaller with molecular weights ranging from 10 to 53 kDa [34]. In comparison, WPI contains proteins varying from 14.2 to 50 kDa, but the main protein (>74 % w/w) is β-lactoglobulin, which has a molecular weight of around 18.2 kDa [42]. Rapeseed lecithin was included, which mainly comprises of phospholipids, which are low molecular weight surfactants. These materials were selected based on their distinct behavior in the nonlinear regime, as shown in our previous work [36].

When comparing the responses of these four stabilizers, we see significant nonlinearity in their overall response. But the origin of the nonlinearities is clearly different. For the WPI-stabilized interface, we see a rhomboidal plot for τ_1 + τ_2 with minor hardening at maximum strain, while this stress contribution has an ellipsoidal shape for pea globulin and pea albumin. So, network disruption clearly does not play a major role in the latter two interfaces. The slope for τ_1 for the pea-albumin interface at 30 % deformation is also higher than that for WPI and pea-globulin, indicating that the former interface has retained more of its network stiffness. The contribution of τ_2 is also more significant for pea-albumin, based on the wider loop we observe in Fig. 6J. But the biggest difference for pea-albumin is observed in the even harmonics: first, τ_4 of pea albumin has the most significant vertical (negative) shift; and its τ_3 contribution has the widest loop, indicating a significant dissipative contribution in the even harmonics. The nonlinearities in the overall loop (of pea albumin) are dominated by the even harmonics and are related to changes in surface density rather than network disruptions. The lecithin stabilized interface shows hardly any vertical shift in τ_4. Here, the dynamic state we are oscillating around has a surface tension that is close to the surface tension of a non-deformed interface in equilibrium. The stress τ_4 also has a relatively higher contribution to the total stress for lecithin, compared to the other stabilizers. There are some minor nonlinearities in the odd harmonics, but again the even harmonics dominate the nonlinearity in the overall stress. We see that the GSD allows us to differentiate between responses of various samples more clearly. But so far, we have done this only on a qualitative level. For LAOS results in bulk rheological measurements, several measures were defined to quantify Lissajous plots, such as stiffening factors, or energy dissipation ratios [26]. In the next section we will introduce similar measures for the four stresses resulting from the GSD in LAOD measurements.

4.4. Quantification of Lissajous plots

We will now quantify the contributions from τ_1 – τ_4, based on their Fourier series, and show how the introduced parameters can be visualized in the Lissajous plots. The slope of the curve for τ_1 is a measure for the stiffness of the interfacial network and represents a (contribution to) dilatational storage modulus. When higher odd harmonics are negligible, τ_1 is a straight line and this modulus is a constant, independent of intracycle strain. But when higher odd harmonics are present in the response, like for example in the response of the WPI-stabilized interface, the slope of the τ_1 curve is not constant. By analogy with [26], we define two new moduli based on τ_1. We define $E_{\tau 1L}$ as the secant modulus associated with τ_1, and as shown in Fig. 7, it is the slope of the curve that connects the origin with the stress at maximum extension. From the Fourier coefficients, it can be calculated as:

$$E_{\tau 1L} = \frac{\tau_1}{\varepsilon}\Big|_{\varepsilon=\pm\varepsilon_0} = \frac{\sum_{k=0}^{n} b'_{2k+1}(-1)^k}{\varepsilon_0} \tag{14}$$

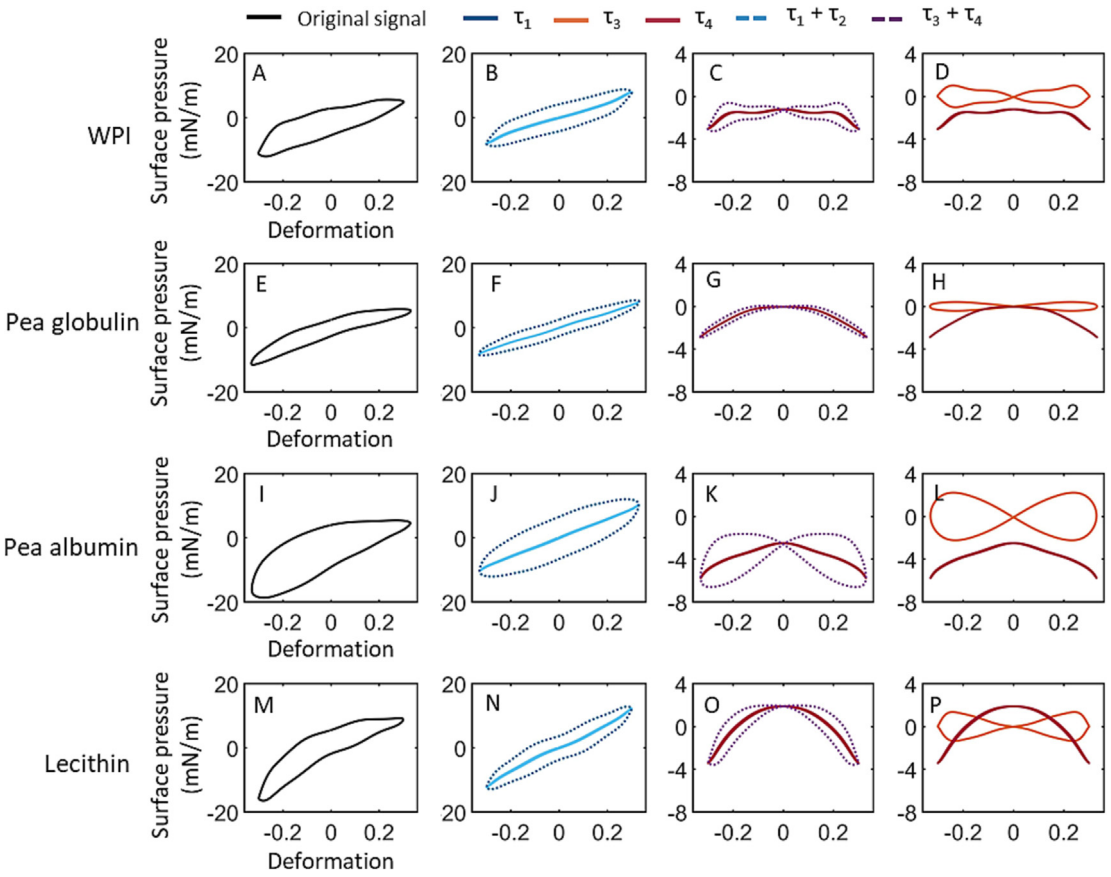

Fig. 6. The total stress at 30 % deformation is shown in plot A, E, I, and M (black); τ_1 (blue, line) and $\tau_1 + \tau_2$ (blue, dashed) in plot B, F, J, and N; τ_4 (red, line) and $\tau_3 + \tau_4$ (purple, dashed) in plot C, G, K, and O; τ_3 (orange, line) and τ_4 (purple, line) in plot D, H, L, and P. (For interpretation of the references to colour in this figure legend, the reader is referred to the web version of this article.)

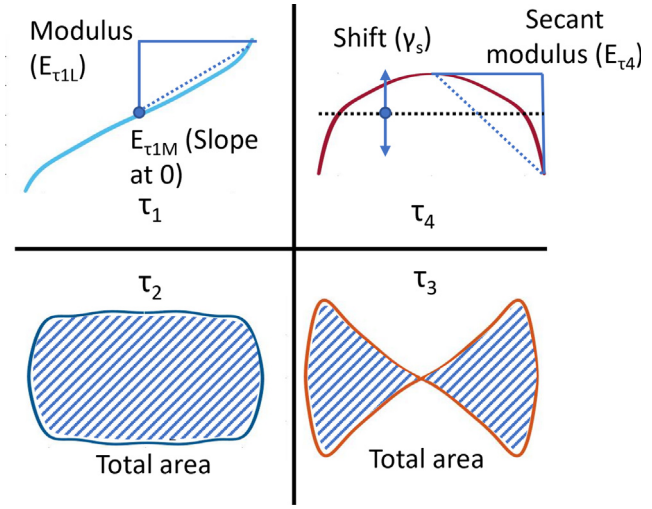

Fig. 7. For τ_1 the quantification is based on the slope at zero deformation and maximum deformation, as described by Eq. (14). The modulus at zero strain is indicated with $E_{\tau 1M}$. For τ_2 and τ_3 quantification is based on the enclosed area of the Lissajous plot. Quantification of τ_4 is based on a secant modulus (the slope of the dashed curve connecting the stress at zero and maximum deformation (see Eq. (17)), and on the vertical shift of the plot.

To quantify intracycle strain stiffening, a modulus at zero deformation ($E_{\tau 1M}$) is defined, also shown in Fig. 7. $E_{\tau 1M}$ can be determined from τ_1 (Eq. (4)) and the strain $\varepsilon(t) = \varepsilon_0 \sin(\omega t)$, by taking the derivative of this stress with respect to the deformation, at zero strain:

$$E_{\tau 1M} = \left.\frac{d\tau_1}{d\varepsilon}\right|_{\varepsilon=0} = \frac{\sum_{k=0}^{n}(2k+1)b'_{2k+1}}{\varepsilon_0} \tag{15}$$

The moduli $E_{\tau 1M}$ and $E_{\tau 1L}$ can then be used for the calculation of the S-factor for intracycle strain hardening:

$$S = \frac{E_{\tau 1L} - E_{\tau 1M}}{E_{\tau 1L}} \tag{16}$$

These moduli and the associated stiffening factor are comparable to the parameters defined for Lissajous plots in shear and dilatational rheology [13,26].

For the elastic stress τ_4 we can also define a secant-type modulus, as illustrated in Fig. 7, and this modulus is the slope of the dashed curve in the plot for τ_4. This modulus can be calculated from Eq. (7), yielding

$$E_{\tau 4} = \frac{\tau_4(\varepsilon_0) - \tau_4(0)}{\varepsilon_0} = \frac{\sum_{k=0}^{n} d'_{2k}\left((-1)^k - 1\right)}{\varepsilon_0} = -\frac{\sum_{k=0}^{n} 2d'_{4k+2}}{\varepsilon_0} \tag{17}$$

The Lissajous plots of τ_4 also show a shift, which we previously identified as an indication we are oscillating around a dynamic state that deviates from the equilibrium state. This shift, γ_s, can be quantified as the 0th harmonic of the Fourier series yielding

$$\gamma_s = d\prime_0 \tag{18}$$

We can also calculate the dissipated energy in the loops of τ_2 and τ_3 ($U_{d\tau 2}$ and $U_{d\tau 3}$), which are equal to the total surface area enclosed by the stress versus strain plots. The dissipated energy per cycle is equal to (using Eq. (5) & Eq. (6))

$$U_{d\tau 2} = \oint \tau_2(t)\dot{\gamma}(t)dt = \pi\varepsilon_0^2 E_1'' \tag{19}$$

$$U_{d\tau 3} = \oint \tau_3(t)\dot{\gamma}(t)dt = 2\varepsilon_0^2 \sum_{k=1}^{n}\left(\frac{E_{2k\tau 3} * k}{k^2 - 1/4}\right) \tag{20}$$

Here $E_1'' = b'_1/\varepsilon_0$ is the loss modulus from the first harmonic of the Fourier series, and $E_{2k\tau 3}$ is the loss modulus of the even harmonics from the Fourier series ($E_{2k\tau 3} = c'_{2k}/\varepsilon_0$). The dissipated energy for τ_2 (Eq. (19)) is the 2D equivalent of the work per unit volume in a shear experiment as calculated by Ganeriwala & Rotz (1987) [43].

The moduli of τ_1 & τ_4 are plotted in Fig. 8 A & B for all interfaces. WPI-stabilized interfaces (Fig. 8 A) show a steep decrease in $E_{\tau 1L}$, from a value close to 80 mN/m at 4 % deformation to around 20 mN/m at 60 % deformation. This indicates a significant breakdown of the interfacial network with increasing amplitude. Pea albumins show a comparable decrease of $E_{\tau 1L}$ up to a strain of about 15 % but retain a somewhat higher modulus in the strain range of 15–30 %, compared to WPI. Again this behavior indicates strong in-plane interactions, which result in network formation, and this network is gradually disrupted and partially broken down with increasing amplitude (LAOD). Pea globulin- and lecithin-stabilized interfaces have relatively low values for $E_{\tau 1L}$, which are nearly constant over the applied strain range. The values for pea-globulin are significantly lower than those of pea-albumin, which was confirmed in previous studies [34]. The lower values for this modulus for globulin and lecithin-stabilized interfaces suggest weaker in-plane interactions among adsorbed interfacial stabilizers, resulting in an interfacial network which is less stiff and more stretchable.

The elastic modulus $E_{\tau 4}$ (Fig. 8 B) is increasingly negative for all interfaces, indicating a more significant contribution of surface density changes, due to (partially) irreversible absorption (on the timescale of a single oscillation cycle). The error margins are relatively large, as τ_4 has a relatively small contribution to the original signal, and a low signal-to-noise ratio impairs the analysis. However, there are still relative differences between the interfaces. A remarkable finding is the $E_{\tau 4}$ of −17 mN/m of lecithin at 30 % deformation, which is significantly lower than for the other interfaces. As we have shown before, the even harmonics which contribute to τ_4 account for nonlinearities in the equation of state of the interface. Lecithin consists mainly of phospholipids, and these

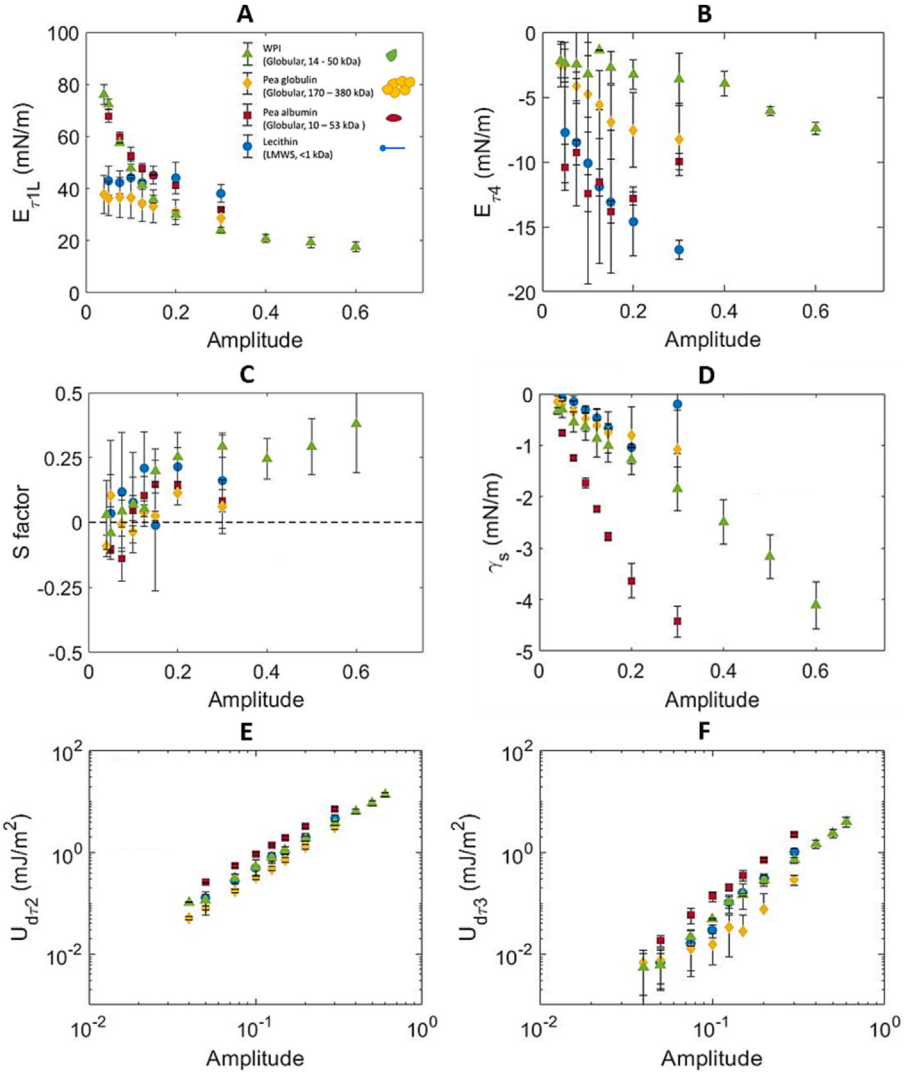

Fig. 8. The modulus of τ_1 (A), modulus of τ_4 (B), strain stiffening factor of τ_1 (C, as defined by Eq. (16)), vertical shift (γ_s) of τ_4 (D), dissipated energy of τ_2 (E), and dissipated energy of τ_3 (F) versus amplitude of deformation for WPI-, pea globulin-, pea albumin-, and lecithin-stabilized interfaces. In plot A, the inset illustrates the main structural difference between the surface-active molecules, with molecular weights of pea albumin and β-lactoglobulin (WPI) as reported by respectively [34,42].

are known to have a complex in-plane phase behavior, which results in an equally complex behavior in the surface pressure-area isotherm. For WPI and pea globulins, this isotherm is much smoother as shown for WPI and pea globulin by [44,45], and hence their values for $E_{\tau 4}$ are less negative.

In Fig. 8 C, the S factor of τ_1 was calculated according to Eq. (16). The S factor for pea albumin-, pea globulin- and lecithin-stabilized interfaces is close to 0 during the amplitude sweep, indicating no intracycle strain hardening. WPI-stabilized interfaces do show an increase in S-value, especially at large amplitudes (>20 %). This could correspond to the stretching of remaining clusters on the WPI-stabilized interface. For other interfacial films, no major differences were found at deformation up to 30 %.

The dissipated energy associated with τ_2 and τ_3 are plotted versus strain in Fig. 8 E and F, respectively. The albumin-stabilized interfaces showed the highest dissipated energy for τ_2. A possible explanation for this could be that after partial disruption of the in-plane network, the residual structure has a higher viscosity than, for example, the WPI-stabilized interface. Alternatively, albumins are small proteins, and the increased dissipation could also come from a contribution from diffusional exchange to the first harmonic. Also, for τ_3, the dissipated energy is higher for albumin, which indicates that diffusional exchange is apparently important in this sample. Pea globulin has the lowest values for the dissipated energy associated with τ_2 and τ_3. This confirms the weak network formation and points to limited diffusional exchange during deformation. The latter is in line with the fact that globulins tend to be large (aggregated) proteins, which diffuse slowly to and from the interface.

Finally, we quantified the shift of τ_4 (see Fig. 8 D), which is calculated from the 0th harmonic of the Fourier series by Eq. (18). A remarkable finding is a much bigger shift for pea albumin than the other interfaces, up to amplitudes of 30 %. The way these experiments are typically performed, is that after droplet formation, the interface is first allowed to reach a (near) equilibrium state (we use "near" here since in most experiments, a true equilibrium state is often not reached on a timescale of a few hours, and the surface tension keeps on decreasing very slowly over time). After this initial phase, when we have reached a quasi-equilibrium surface tension, γ_{eq}, we start the oscillations. As we noted before, the shift γ_s, implies that during oscillation, we are oscillating not around γ_{eq}, but around a nonequilibrium state of the interface, for which the surface tension is higher than γ_{eq} (Since according to Eq. (1), a shift to lower values for Π, indicates a higher value for γ_0). This shift in γ_0 is apparently much higher for albumin than for the other components.

We see that the GSD allows us to distinguish much better between the samples studied here and allows us to quantify these differences. There is one additional advantage of this approach. So far, LAOD studies on interfaces have been limited to the study of elastic Lissajous plots, so the plots of surface pressure versus strain. However, in the highly nonlinear regime, it can also be advantageous to study the viscous Lissajous plots, i.e., the plots of surface pressure versus strain rate ($\dot{\gamma}$). In shear experiments, this can provide additional information on flow behavior, after yielding of a structure, and allows for the quantification of possible shear thinning in that behavior. Since the GSD gives us all the Fourier coefficients of the response (up to order 10 here), it is straightforward to also construct the viscous plots for LAOD experiments. This is, of course, useful only when there are significant contributions from the higher odd harmonics (evident from the rhomboidal shape of the elastic Lissajous plot). Here, this shape was observed only for WPI interfaces, and for this interface the viscous plot is shown in Fig. 9 at 60 % deformation. Note that since we are now plotting stresses against strain rate, τ_2 is now a line instead of a closed loop. Around $\dot{\gamma} = 0$, the blue curve has a finite slope, so viscosity is finite, whereas in the extremes at $\dot{\gamma} = \pm 0.075$, the viscous stress curve is nearly horizontal, creating a sigmoidal curve (Fig. 9 B). The sigmoidal shape shows that there is shear thinning behavior in τ_2 at 60 % deformation. This stress contribution shows nicely that LAOD experiments can (partially) disrupt the interfacial microstructure, causing flow of the surface-active components.

Although the even harmonic terms have an energy storage (τ_4) and dissipative component (τ_3), these are not deviatoric stresses and depend only on the magnitude of the applied strain. Therefore, in their strain rate plot in Fig. 9 C, τ_4 is still represented by a line, and τ_3 by a loop.

5. Conclusions

In this study, we discussed a general stress decomposition (GSD) for the analysis of interfacial stress responses in large amplitude oscillatory dilatation. The GSD is a framework comparable to the decomposition for shear responses that was developed by Ewoldt et al. [26]. Here, we applied this framework to dilatational responses and introduced several new quantitative measures to analyze this decomposition. We illustrated the framework by applying it to responses of interfaces stabilized by several proteins and phospholipids.

We expected the stress in dilatation to be a function of contributions from network deformations and surface density changes of the emulsifier. To prove this we decomposed the surface stress into four contributions (τ_1 - τ_4), representing an elastic and viscous contribution to the total stress from the odd Fourier harmonics, and a viscous and elastic contribution from the even harmonics.

The decomposition is especially relevant for nonlinear-responses, which can contain in-plane viscoelastic stresses and anisotropic effects, as described by the surface extra stress tensor in the jump surface momentum balance [1,39,46]. We studied

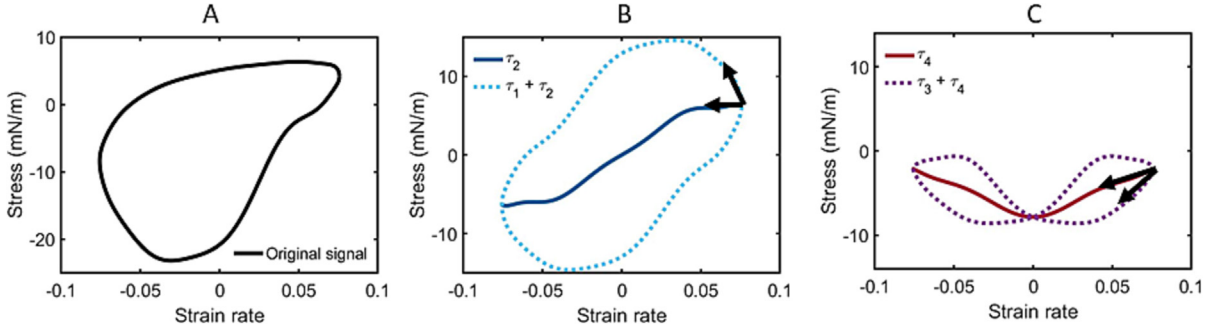

Fig. 9. WPI-stabilized interface at 60 % deformation plotted versus the strain rate, with the original signal (A, black) and its components $\tau_1 + \tau_2$ (blue, dashed) & τ_2 (blue, line) (B) and $\tau_3 + \tau_4$ (purple, dashed) & τ_4 (red, line) (C). (For interpretation of the references to colour in this figure legend, the reader is referred to the web version of this article.)

the dilatational response of WPI-, pea albumin-, pea globulin- and rapeseed lecithin-stabilized air–water interfaces in terms of these four stress contributions and found fundamental differences between the responses of these interfaces. Until now, dilatational responses could only be quantified from the overall response, whereas our decomposition provides quantification of the underlying physical mechanisms. The response of all interfaces was dominated by the odd harmonics (incorporated in τ_1 and τ_2) at small deformations (linear regime). The contribution from even harmonics (incorporated in τ_3 and τ_4) became more prevalent at large deformations in the nonlinear regime, as Lissajous plots became more asymmetric. The higher odd harmonics in τ_1 and τ_2, are most likely related to partial disruptions of the interfacial network, based on the similarities with interfacial shear rheology. The stresses τ_3 and τ_4 are related to surface density changes at the interfaces during deformation, and account for the nonlinearities in the equation of state of the interface.

We introduced several new measures (moduli and dissipated energies) to quantify the contributions of $\tau_1 - \tau_4$, resulting in a deeper understanding of the dilatational responses as shown for WPI-, pea albumin-, pea globulin-, and rapeseed lecithin-stabilized interfaces. GSD provides a framework for decomposition of asymmetric nonlinear responses. which can be applied to any interface that is subjected to dilatational deformations. Moreover we provided physical interpretation of each contribution that will help explain the nonlinear behavior of complex interfaces for multicomponent systems, highly relevant for application in agriculture, foods, cosmetics, and pharmacology [1–3]. To facilitate the use we developed a MATLAB app for performing GSD which is available upon request by contacting the corresponding author.

Data availability

Data will be made available on request.

Declaration of Competing Interest

The authors declare that they have no known competing financial interests or personal relationships that could have appeared to influence the work reported in this paper.

Acknowledgements

This publication is part of the 'Animal-free milk proteins' project (with project number NWA.1292.19.302) of the NWA research programme 'Research along Routes by Consortia (ORC)', which is funded by the Dutch Research Council (NWO).

References

[1] L.M.C. Sagis, Dynamic properties of interfaces in soft matter: Experiments and theory, Rev Mod Phys. 83 (2011) 1367–1403, https://doi.org/10.1103/RevModPhys.83.1367.
[2] L.M.C. Sagis, Dynamics of controlled release systems based on water-in-water emulsions: A general theory, Journal of Controlled Release. 131 (2008) 5–13, https://doi.org/10.1016/j.jconrel.2008.07.010.
[3] C.D. Ampatzidis, E.-M.-A. Varka, T.D. Karapantsios, Interfacial activity of amino acid-based glycerol ether surfactants and their performance in stabilizing O/W cosmetic emulsions, Colloids Surf A Physicochem Eng Asp. 460 (2014) 176–183, https://doi.org/10.1016/j.colsurfa.2014.02.033.
[4] R. Miller, J.K. Ferri, A. Javadi, J. Krägel, N. Mucic, R. Wüstneck, Rheology of interfacial layers, Colloid Polym Sci. 288 (2010) 937–950, https://doi.org/10.1007/s00396-010-2227-5.
[5] D. Langevin, Influence of interfacial rheology on foam and emulsion properties, Adv Colloid Interface Sci. 88 (2000) 209–222, https://doi.org/10.1016/S0001-8686(00)00045-2.
[6] Y. Jin, D. Liu, J. Hu, Effect of Surfactant Molecular Structure on Emulsion Stability Investigated by Interfacial Dilatational Rheology, Polymers (Basel). 13 (2021) 1127, https://doi.org/10.3390/polym13071127.
[7] Y. Tian, Z. Zhang, A. Taha, Y. Chen, H. Hu, S. Pan, Interfacial and emulsifying properties of β-conglycinin/pectin mixtures at the oil/water interface: Effect of pH, Food Hydrocoll. 109 (2020), https://doi.org/10.1016/j.foodhyd.2020.106145 106145.
[8] F. Zhan, J. Hu, C. He, J. Sun, J. Li, B. Li, Complexation between sodium caseinate and gallic acid: Effects on foam properties and interfacial properties of foam, Food Hydrocoll. 99 (2020), https://doi.org/10.1016/j.foodhyd.2019.105365 105365.
[9] D. Peng, W. Jin, P. Zhou, C. Ren, B. Li, Foaming and surface rheological behaviors of gliadin particles: Effect of solvent and concentration of gliadin stock solution, Food Hydrocoll. 106 (2020), https://doi.org/10.1016/j.foodhyd.2020.105868 105868.
[10] S. Böttcher, J.K. Keppler, S. Drusch, Mixtures of Quillaja saponin and beta-lactoglobulin at the oil/water-interface: Adsorption, interfacial rheology and emulsion properties, Colloids Surf A Physicochem Eng Asp. 518 (2017) 46–56, https://doi.org/10.1016/j.colsurfa.2016.12.041.
[11] F. Zhan, J. Li, M. Shi, D. Wu, B. Li, Foaming Properties and Linear and Nonlinear Surface Dilatational Rheology of Sodium Caseinate, Tannin Acid, and Octenyl Succinate Starch Ternary Complex, J Agric Food Chem. 67 (2019) 2340–2349, https://doi.org/10.1021/acs.jafc.8b06356.
[12] F. Zhan, Y. Chen, J. Hu, M. Youssef, A. Korin, J. Li, B. Li, Combining surface dilatational rheology and quantitative proteomics as a tool for understanding microstructures of air/water interfaces stabilized by sodium caseinate/tannic acid complex, Food Hydrocoll. 102 (2020), https://doi.org/10.1016/j.foodhyd.2019.105627 105627.
[13] S.E.H.J. Van Kempen, H.A. Schols, E. Van Der Linden, L.M.C. Sagis, Non-linear surface dilatational rheology as a tool for understanding microstructures of air/water interfaces stabilized by oligofructose fatty acid esters, Soft Matter. 9 (2013) 9579–9592, https://doi.org/10.1039/c3sm51770e.
[14] L.M.C. Sagis, K.N.P. Humblet-Hua, S.E.H.J. Van Kempen, Nonlinear stress deformation behavior of interfaces stabilized by food-based ingredients, Journal of Physics Condensed Matter. 26 (2014), https://doi.org/10.1088/0953-8984/26/46/464105.
[15] G. Giménez-Ribes, M. Habibi, L.M.C. Sagis, Interfacial rheology and relaxation behavior of adsorption layers of the triterpenoid saponin Escin, J Colloid Interface Sci. 563 (2020) 281–290, https://doi.org/10.1016/j.jcis.2019.12.053.
[16] J. Yang, I. Thielen, C.C. Berton-Carabin, E. van der Linden, L.M.C. Sagis, Nonlinear interfacial rheology and atomic force microscopy of air-water interfaces stabilized by whey protein beads and their constituents, Food Hydrocoll. 101 (2020), https://doi.org/10.1016/j.foodhyd.2019.105466 105466.
[17] J. Yang, I. Faber, C.C. Berton-Carabin, C.V. Nikiforidis, E. van der Linden, L.M.C. Sagis, Foams and air-water interfaces stabilised by mildly purified rapeseed proteins after defatting, Food Hydrocoll. 703 (2020), https://doi.org/10.1016/j.foodhyd.2020.106270 106270.
[18] L. Seta, N. Baldino, D. Gabriele, F.R. Lupi, B. de Cindio, Rheology and adsorption behaviour of β-casein and β-lactoglobulin mixed layers at the sunflower oil/water interface, Colloids Surf A Physicochem Eng Asp. 441 (2014) 669–677, https://doi.org/10.1016/j.colsurfa.2013.10.041.
[19] J. Yang, A. de Wit, C.F. Diedericks, P. Venema, E. van der Linden, L.M.C. Sagis, Foaming and emulsifying properties of extensively and mildly extracted Bambara groundnut proteins: A comparison of legumin, vicilin and albumin protein, Food Hydrocoll. 123 (2022), https://doi.org/10.1016/j.foodhyd.2021.107190 107190.
[20] L.M.C. Sagis, P. Fischer, Nonlinear rheology of complex fluid-fluid interfaces, Curr Opin Colloid, Interface Sci. 19 (2014) 520–529, https://doi.org/10.1016/j.cocis.2014.09.003.
[21] V. Sharma, A. Jaishankar, Y.C. Wang, G.H. McKinley, Rheology of globular proteins: Apparent yield stress, high shear rate viscosity and interfacial viscoelasticity of bovine serum albumin solutions, Soft Matter. 7 (2011) 5150–5160, https://doi.org/10.1039/c0sm01312a.
[22] L.G. Cascão Pereira, O. Théodoly, H.W. Blanch, C.J. Radke, Dilatational rheology of BSA conformers at the air/water interface, Langmuir. 19 (2003) 2349–2356, https://doi.org/10.1021/la020720e.
[23] R.H. Ewoldt, A.E. Hosoi, G.H. McKinley, An ontology for large amplitude oscillatory shear flow, AIP Conf Proc. 1027 (2008) 1135–1137, https://doi.org/10.1063/1.2964492.
[24] P. Erni, A. Parker, Nonlinear Viscoelasticity and Shear Localization at Complex Fluid Interfaces, Langmuir. 28 (2012) 7757–7767, https://doi.org/10.1021/la301023k.
[25] R.H. Ewoldt, P. Winter, J. Maxey, G.H. McKinley, Large amplitude oscillatory shear of pseudoplastic and elastoviscoplastic materials, Rheol Acta. 49 (2010) 191–212, https://doi.org/10.1007/s00397-009-0403-7.
[26] R.H. Ewoldt, A.E. Hosoi, G.H. McKinley, New measures for characterizing nonlinear viscoelasticity in large amplitude oscillatory shear, J Rheol (N Y N Y). 52 (2008) 1427–1458, https://doi.org/10.1122/1.2970095.
[27] A.G. Bykov, L. Liggieri, B.A. Noskov, P. Pandolfini, F. Ravera, G. Loglio, Surface dilational rheological properties in the nonlinear domain, Adv Colloid Interface Sci. 222 (2015) 110–118, https://doi.org/10.1016/j.cis.2014.07.006.
[28] K.S. Cho, K. Hyun, K.H. Ahn, S.J. Lee, A geometrical interpretation of large amplitude oscillatory shear response, J Rheol (N Y N Y). 49 (2005) 747–758, https://doi.org/10.1122/1.1895801.
[29] A.J. Giacomin, J.M. Dealy, Large-Amplitude Oscillatory Shear, in: Techniques in Rheological Measurement, Springer Netherlands, Dordrecht, 1993: pp. 99–121. https://doi.org/10.1007/978-94-011-2114-9_4.

[30] K. Hyun, S.H. Kim, K.H. Ahn, S.J. Lee, Large amplitude oscillatory shear as a way to classify the complex fluids, J Nonnewton Fluid Mech. 107 (2002) 51–65, https://doi.org/10.1016/S0377-0257(02)00141-6.
[31] W. Yu, P. Wang, C. Zhou, General stress decomposition in nonlinear oscillatory shear flow, J Rheol (N Y N Y). 53 (2009) 215–238, https://doi.org/10.1122/1.3037267.
[32] P.A. Rühs, C. Affolter, E.J. Windhab, P. Fischer, Shear and dilatational linear and nonlinear subphase controlled interfacial rheology of β-lactoglobulin fibrils and their derivatives, J Rheol (N Y N Y). 57 (2013) 1003–1022, https://doi.org/10.1122/1.4802051.
[33] P.A. Rühs, N. Scheuble, E.J. Windhab, P. Fischer, Protein adsorption and interfacial rheology interfering in dilatational experiment, European Physical Journal: Special Topics. 222 (2013) 47–60, https://doi.org/10.1140/epjst/e2013-01825-0.
[34] R. Kornet, J. Yang, P. Venema, E. van der Linden, L.M.C. Sagis, Optimizing pea protein fractionation to yield protein fractions with a high foaming and emulsifying capacity, Food Hydrocoll. 126 (2022), https://doi.org/10.1016/j.foodhyd.2021.107456 107456.
[35] X. Zhou, G. Sala, L.M.C. Sagis, Bulk and interfacial properties of milk fat emulsions stabilized by whey protein isolate and whey protein aggregates, Food Hydrocoll. 109 (2020), https://doi.org/10.1016/j.foodhyd.2020.106100 106100.
[36] J. Yang, L.C. Waardenburg, C.C. Berton-Carabin, C.V. Nikiforidis, E. van der Linden, L.M.C. Sagis, Air-water interfacial behaviour of whey protein and rapeseed oleosome mixtures, J Colloid Interface Sci. 602 (2021) 207–221, https://doi.org/10.1016/j.jcis.2021.05.172.
[37] J. Yang, S.P. Lamochi Roozalipour, C.C. Berton-Carabin, C.V. Nikiforidis, E. van der Linden, L.M.C. Sagis, Air-water interfacial and foaming properties of whey protein - sinapic acid mixtures, Food Hydrocoll. 112 (2021), https://doi.org/10.1016/j.foodhyd.2020.106467 106467.
[38] A.J. Giacomin, J.M. Dealy, Large-Amplitude Oscillatory Shear, in: Techniques in Rheological Measurement, Springer, Netherlands, Dordrecht, 1993, pp. 99–121, https://doi.org/10.1007/978-94-011-2114-9_4.
[39] L.M.C. Sagis, Dynamic surface tension of complex fluid-fluid interfaces: A useful concept, or not?, European Physical Journal: Special Topics 222 (2013) 39–46, https://doi.org/10.1140/epjst/e2013-01824-1.
[40] M.E.H. van den Berg, S. Kuster, E.J. Windhab, L.M.C. Sagis, P. Fischer, Nonlinear shear and dilatational rheology of viscoelastic interfacial layers of cellulose nanocrystals, Physics of Fluids. 30 (2018), https://doi.org/10.1063/1.5035334 072103.
[41] L.M.C. Sagis, M. Ramaekers, E. van der Linden, Constitutive equations for an elastic material with anisotropic rigid particles, Phys Rev E Stat Nonlin Soft Matter Phys. 63 (2001) 515041–515048, https://doi.org/10.1103/PhysRevE.63.051504.
[42] C.I. Butré, P.A. Wierenga, H. Gruppen, Effects of ionic strength on the enzymatic hydrolysis of diluted and concentrated whey protein isolate, J Agric Food Chem. 60 (2012) 5644–5651, https://doi.org/10.1021/jf301409n.
[43] S.N. Ganeriwala, C.A. Rotz, Fourier transform mechanical analysis for determining the nonlinear viscoelastic properties of polymers, Polym Eng Sci. 27 (1987) 165–178, https://doi.org/10.1002/pen.760270211.
[44] M. Subirade, J. Gueguen, K.D. Schwenke, Effect of dissociation and conformational changes on the surface behavior of pea legumin, J Colloid Interface Sci. 152 (1992) 442–454, https://doi.org/10.1016/0021-9797(92)90045-N.
[45] J.M. Rodríguez Patino, M.R.R. Niño, C.C. Sánchez, M.C. Fernández, Whey protein isolate-monoglyceride mixed monolayers at the air-water interface. Structure, morphology, and interactions, Langmuir. 17 (2001) 7545–7553, https://doi.org/10.1021/la0102814.
[46] J.C. Slattery, L. Sagis, E.-S. Oh, Interfacial Transport Phenomena, Springer, US, Boston, MA (2007), https://doi.org/10.1007/978-0-387-38442-9.